Charge-stripe order, antiferromagnetism, and spin dynamics in the cuprate-analog nickelate La$_4$Ni$_3$O$_8$

O. O. Bernal,[1,*] D. E. MacLaughlin,[2] G. D. Morris,[3] P.-C. Ho,[4] Lei Shu,[5] C. Tan,[5]
J. Zhang,[5,†] Z. Ding,[5] K. Huang,[5,‡] and V. V. Poltavets[6]

[1]*Department of Physics and Astronomy, California State University, Los Angeles, California 90032, USA*
[2]*Department of Physics and Astronomy, University of California, Riverside, California 92521, USA*
[3]*Centre for Molecular and Materials Science, TRIUMF, Vancouver, British Columbia, Canada V6T 2A3*
[4]*Department of Physics, California State University, Fresno, California 93740,USA*
[5]*State Key Laboratory of Surface Physics, Department of Physics, Fudan University, Shanghai 200433, China*
[6]*Department of Chemistry and Advanced Materials Research Institute, University of New Orleans, New Orleans, Louisiana 70148, USA*

We report results of a muon spin rotation (μSR) study of the cuprate-analog nickelate La$_4$Ni$_3$O$_8$, which undergoes a transition at 105 K to a low-temperature phase with charge-stripe and antiferromagnetic (AFM) order on square planar NiO$_2$ layers. Zero-field μSR shows that the AFM transition is abrupt, commensurate, and has a quasi-two-dimensional character below $\sim$25 K. Comparison of observed muon precession frequencies with Ni dipolar field calculations yields Ni moments $\lesssim 0.5\,\mu_B$. Dynamic muon spin relaxation above 105 K suggests critical slowing of Ni spin fluctuations, but is inconsistent with corresponding ^{139}La NMR results. Critical slowing and an abrupt transition are also observed in the planar cuprate AFM La$_2$CuO$_{4+\delta}$, where they are taken as evidence for weakly interplanar-coupled two-dimensional AFM spin fluctuations, but our μSR data do not agree quantitatively with theoretical predictions for this scenario when applied to the nickelate.

I. INTRODUCTION

Bednorz and Müller searched for superconductivity in nickel-based systems without success before they discovered superconducting La$_2$BaCuO$_{4+\delta}$ [1]. For many years after, high-T_c superconductivity was found only in cuprate compounds with CuO$_2$-layered structures. It is now well known that aside from the cuprates other layered systems (e.g., Fe-pnictide/chalcogenide and BiS$_2$-based materials) also become superconductors, suggesting a potential universality in layered superconductivity. This in turn revives interest in the quest for Cu-analog, Ni-based, superconducting materials. The motivation for studying these materials lies in their potential to help answer current experimental and theoretical questions regarding superconductivity in layered compounds, to assess the universality of layer superconductivity, and to provide clues for where to search for new layered superconductors.

The trilayer T'-type nickelate La$_4$Ni$_3$O$_8$ [2,3] is one such material. The crystal structure of this compound involves square planar NiO$_2$ trilayers, isoelectronic to the Cu^{2+}O$_2$ layers of the cuprates if the Ni valence were 1+. Further interest in comparing these systems arises from an antiferromagnetic (AFM) phase transition in La$_4$Ni$_3$O$_8$ at a Néel temperature $T_N = 105$ K into a state with commensurate spin and charge stripes [4–6], similar in some respects to the AFM transition

occurring in the cuprates. A charge-stripe/spin-stripe phase has been observed in the T-type nickelate La$_{5/3}$Sr$_{1/3}$NiO$_4$ [7] which, like La$_4$Ni$_3$O$_8$, is $\frac{1}{3}$ hole doped.

This paper reports a muon spin rotation and relaxation (μSR) study of the magnetic structure and spin dynamics of La$_4$Ni$_3$O$_8$. μSR is a magnetic resonance technique [8], conceptually similar to NMR, that uses muon spins implanted into the sample as microscopic probes of their static and dynamic magnetic environment. We find that the 105-K transition is abrupt (discontinuous to within experimental resolution), and that the commensurate AFM configuration is consistent with both magnetic and charge-stripe order as found in x-ray [5] and neutron [6] diffraction studies, respectively. Observed spectra of muon spin precession frequencies resemble histograms of calculated Ni dipolar fields at candidate muon sites for specific AFM stripe configurations, with reduced Ni moments 0.4–0.5 μ_B. We present μSR evidence that the magnetic transition at T_N is quasi-two-dimensional (quasi-2D) in nature, in which the trilayers are ordered but fluctuate independently down to $\sim$25 K. Below this temperature, three-dimensional (3D) static magnetism is observed, with disorder along the normal to the trilayer planes as found by neutron diffraction [6].

Dynamic muon spin relaxation in the paramagnetic phase suggests critical slowing of Ni spin fluctuations with a divergence at $\sim T_N$. This is not expected for two-dimensional (2D) Heisenberg magnets, where the critical behavior is due to 2D spin fluctuations that do not order at finite T [9,10]. In that scenario, the 3D transition is due to a weak interplanar coupling, and does not dominate the critical spin dynamics. Evidence for this 2D criticality in the planar cuprate AFM

---

*Corresponding author: obernal@exchange.calstatela.edu

†Present address: Geballe Laboratory for Advanced Materials, Stanford University, Stanford, California 94305, USA.

‡Present address: Lawrence Livermore National Laboratory, Livermore, California 94550, USA.

$La_2CuO_{4+\delta}$ is found from NMR studies [11]. Our μSR data in $La_4Ni_3O_8$ do not agree quantitatively with this scenario, and instead suggest the possibility of a second-order transition with a very sharp onset at T_N. This is in contrast with the $T = 0$ divergence of the ^{139}La NMR relaxation rate in $La_4Ni_3O_8$ [12], which has been taken as evidence for 2D fluctuations.

The paper is organized as follows: The current understanding of $La_4Ni_3O_8$ and related systems is reviewed in Sec. II, with emphasis on the charge/stripe nature of the 105-K transition. Section III gives experimental details and a brief description of the μSR technique. Candidate muon stopping sites in the crystal are discussed in Sec. IV, and Sec. V reports μSR results in the ordered phase and their interpretation. Section VI reports muon spin relaxation in the paramagnetic phase above 105 K. Our results are discussed in Sec. VII and summarized in Sec. VIII. Appendix A gives supplementary information on AFM configurations, and Appendix B presents a simple model for zero-field μSR at an abrupt magnetic transition with an inhomogeneous distribution of transition temperatures.

II. BACKGROUND

Anisimov, Bukhvalov, and Rice [13] concluded "Only if the Ni ions are forced into a planar coordination with the O ions can a $S = \frac{1}{2}$ magnetic insulator be realized with the difficult Ni^{1+} oxidation state and possibly doped with low spin ($S = 0$) Ni^{2+} holes directly analogous to the superconducting cuprates." That is, a system with electronic configuration Ni^{1+}/Ni^{2+} would have the same configuration as that of Cu^{2+}/Cu^{3+} in the cuprates, but to be a true analog it would also need to be in a square planar coordination with O ions. The Ni^{1+}/Ni^{2+} configuration is rare in oxides but it does exist, and conforms with the condition of Anisimov *et al.* in the T'-type nickelates $Ln_{n+1}Ni_nO_{2n+2}$, Ln = La, Nd, $n = 2, 3$, and ∞ [14]. In this formula n is the number of NiO_2 layers in a multilayer of square-coordinated Ni ions.

Poltavets *et al.* [4] reported a magnetic transition at 105 K for $La_4Ni_3O_8$ ($n = 3$), and attributed it to Ni-spin intertrilayer interactions in analogy with undoped $La_2CuO_{4+\delta}$. No transition was seen in the magnetization for applied fields lower than 0.1 T, but the observed change in slope of the resistivity $\rho(T)$ and the lambda anomaly in the specific heat at 105 K were taken as evidence for a transition in zero field. At low temperatures $\rho(T)$ exhibits semiconducting behavior [4]. ^{139}La NMR measurements indicated that the transition is to an AFM phase (i.e., 105 K is a Néel temperature T_N), further suggesting the possibility of a cuprate analog.

The results of Ref. [4] triggered a good deal of theoretical and experimental work [12,15–20]. Pardo and Pickett [15] predicted an insulating ground state of the Mott type, and related the transition to binding of dz^2 orbitals of Ni ions in outer and middle layers of a trilayer (designated Ni1 and Ni2, respectively). Checkerboard AFM ordering in NiO_2 planes was assumed, although powder neutron diffraction has not yielded specific indications for magnetic order [3,4]. A predicted metal-insulator transition under pressure [15] was not observed [17].

Liu *et al.* [18] and Wu [19] predicted $La_4Ni_3O_8$ to be a C-type AFM using different theoretical methods. A correlation of the metal/insulator character of the system with dimensionality was found from first-principles calculations in $La_{n+1}Ni_nO_{2n+2}$ by Liu *et al.* [21]. The quasi-2D $n = 2$ and 3 varieties were predicted to be molecular insulators in contrast with 3D ($n = \infty$) $LaNiO_2$, which according to their calculated electronic structure is metallic by virtue of Ni-La hybridization. The inclusion of electron correlation effects in first-principles calculations by Patra *et al.* [20] suggested that the two inequivalent Ni1 and Ni2 atoms in the $La_{4-x}Sr_xNi_3O_8$ crystal structure are both in a high-spin state, with an average valence of $+1.33$ independent of x doping.

There were indications, however, that the physics of the nickelates is more complicated than expected. A fit to the temperature dependence of the ^{139}La NMR relaxation rate $1/T_1$ in $La_4Ni_3O_8$ [12] required a Korringa term $1/T_1T =$ const, indicative of a Fermi liquid phase. This is in contrast to the AFM cuprate compounds, which are Mott insulators. In addition, $1/T_1$ in the paramagnetic phase above T_N could be fit as diverging at $T = 0$ [12], rather than at T_N as expected for a second-order (continuous) transition in 3D. A $T = 0$ divergence is characteristic of critical fluctuations of a 2D Heisenberg quantum antiferromagnet [9,10], and is observed in the quasi-2D cuprate antiferromagnet $La_2CuO_{4+\delta}$ [11].

More recently, NMR measurements by ApRoberts-Warren *et al.* [22] in the paramagnetic phase of the bilayer ($n = 2$) T'-type compound $La_3Ni_2O_6$ revealed very similar behavior of the ^{139}La relaxation rate to that found previously in trilayer $La_4Ni_3O_8$. Although they observed no magnetic transition in the bilayer down to 5 K, their results were ascribed to similarity in the electronic structure of the two materials, presumed to be of the 2D variety.

The discussion of the 105-K transition in $La_4Ni_3O_8$ shifted in 2016, when Zhang *et al.* [5] reported results from synchrotron x-ray diffraction measurements on single crystals. They found a quasi-2D stripe-ordered charge configuration below 105 K, with orientation at 45° to the Ni-O-Ni bonds in NiO_2 squares and a 2D supercell $3\sqrt{2}a \times \sqrt{2}a$, where a is the Ni-Ni nearest-neighbor distance. This is similar to the charge order found in $La_{5/3}Sr_{1/3}NiO_4$ [7], a related $\frac{1}{3}$ hole-doped single-layer Ruddlesden-Popper nickelate, where the average Ni valence is 2.33+. The stripe pattern in $La_4Ni_3O_8$ is two Ni^{1+} ($S = \frac{1}{2}$) rows followed by one Ni^{2+} ($S = 0$) row, oriented at 45° to the planar Ni-O bonds, with staggered stacking along the c axis. The 2:1 ratio preserves the formal Ni valence 1.33+. All three layers in a trilayer possess stripes. The magnetic structure was not obtained in this study, which sampled only charge degrees of freedom.

Ab initio calculations by Botana *et al.* [23] yielded stripe charge order from a combination of structural distortion and AFM order, in which Ni^{2+} ions have spin $S = 0$, and Ni^{1+} $S = \frac{1}{2}$ ions order antiferromagnetically, similar to the spin-$\frac{1}{2}$ insulating antiferromagnetism of the cuprate parent materials. In this result, the valences of corresponding Ni1 and Ni2 ions in a trilayer are the same. Two 2D supercells of the observed stripe pattern and the proposed 2D AFM order in a single Ni layer [23] are shown in Fig. 1.

Very recently, Zhang *et al.* [6] reported results of neutron Bragg diffraction experiments on $La_4Ni_3O_8$. Their measurements confirm the magnetic ground state, with stripe AFM order commensurate with the charge stripes in individual

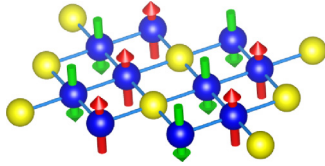FIG. 1. Charge stripe [5] and proposed AFM moment configurations [23] on a nickel layer in $La_4Ni_3O_8$. Blue spheres: Ni^{1+} ions ($S = \frac{1}{2}$). Yellow spheres: Ni^{2+} ions ($S = 0$). Arrows: AFM ordered moments. O^{2-} ions are not shown.

trilayers but little or no correlation between trilayers. In contrast to $La_{5/3}Sr_{1/3}NiO_4$ and to most other transition metal oxides, the charge and spin stripes form simultaneously at 105 K.

III. EXPERIMENT

A. Sample

Polycrystalline $La_4Ni_3O_8$ was prepared as described previously [3] and characterized by powder x-ray diffraction, x-ray absorption spectroscopy, magnetization, specific heat, resistivity, and NMR measurements [3,4,12]. For our μSR experiments we used enough material to fully cover a circular area of about 1 cm in diameter and 1 mm thickness.

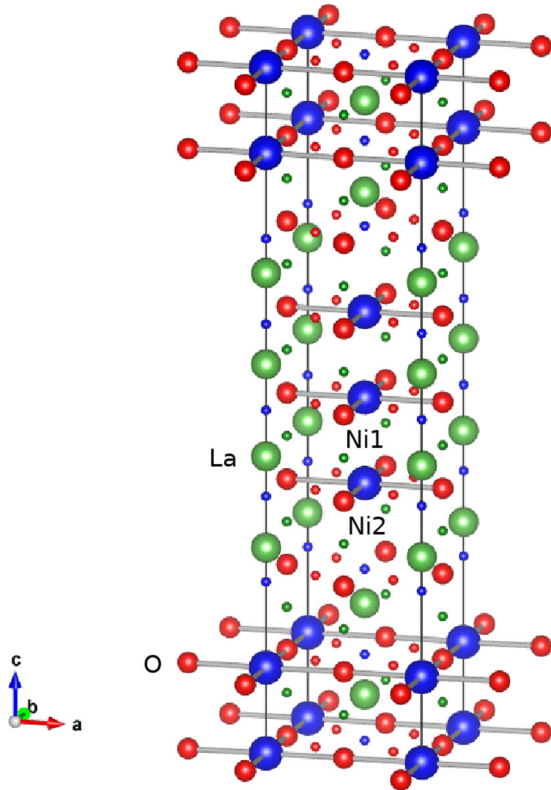The two-trilayer tetragonal unit cell of $La_4Ni_3O_8$ (space group $I4/mmm$, no. 139) is shown in Fig. 2. There are two

FIG. 2. Unit cell of $La_4Ni_3O_8$ (space group $I4/mmm$, no. 139). Blue spheres: Ni; red spheres: O; green spheres: La. Small spheres: candidate muon sites (cf. Sec. IV, Table I). Red: $\mu1$–$\mu3$; green: $\mu4$–$\mu5$; blue: $\mu6$–$\mu8$.

inequivalent Ni sites (Ni1 and Ni2) and three inequivalent oxygen sites, two of which coordinate the Ni ions in the planar NiO_2 layers. The third oxygen sites form separate square-coordinated layers, with La ions above and below the square centers forming flourite La-O blocks that separate and isolate one NiO_2 trilayer from the next. NiO_2 layers within a trilayer are separated by La-only planes. The candidate muon sites shown in Fig. 2 are discussed in Sec. IV.

B. μSR experiments

In the μSR technique [8], 100% spin-polarized muons are implanted into a sample, where they decay [$\mu^\pm \to e^\pm + \nu_e(\overline{\nu}_e) + \overline{\nu}_\mu(\nu_\mu)$] with a mean lifetime 2.197μs. Usually positive muons (μ^+) are used, which stop in interstitial sites.[1] The decay positron is preferentially emitted in the direction of the μ^+ spin at the time of decay. Thus the time-dependent positron count-rate asymmetry $A(t)$ (the *asymmetry spectrum*), where t is the time after implantation, directly yields the time evolution of the ensemble μ^+ spin polarization $G(t)$ [$G(0) \equiv 1$]: $A(t) = A_0 G(t)$, where the initial asymmetry $A_0 = 0.2$–0.3 is instrument dependent. Information on local magnetic behavior is contained in $G(t)$. Measurement of a single asymmetry spectrum typically requires $\gtrsim 10^7$ events.

μ^+SR experiments on $La_4Ni_3O_8$ were carried out with the LAMPF spectrometer at the M20D muon beam line, TRIUMF, Vancouver, Canada, over the temperature range 1.2–300 K, in zero magnetic field (ZF) and in longitudinal applied fields (LF) (field parallel to the initial μ^+ spin polarization) up to 4 kOe. Data were analyzed using the Paul Scherrer Institute MUSRFIT fitting program [24] and the TRIUMF PHYSICA programming environment.[2]

IV. μ^+ STOPPING SITES

μ^+ precession frequencies in ordered magnets yield static magnetic field values at the μ^+ stopping sites, which can help to characterize the magnetic order if these sites are known. Implanted positive muons in oxides are likely to stop near O^{2-} ions, and in $La_4Ni_3O_8$ with stripe order the large unit cell yields a considerable number of such candidate sites. To date, there are no reported calculations of site locations or relative occupations in $La_4Ni_3O_8$ using, for example, density functional theory (DFT) theory [25].

In lieu of such information, we consider candidate μ^+ sites that are symmetric with respect to oxygen near neighbors. Eight such sites that are crystallographically inequivalent are shown in Fig. 2 and listed in Table I. It is customary [5,6,16,23] to describe magnetic and stripe structure in $La_4Ni_3O_8$ using the setting $F4/mmm$, in which basal-plane unit vectors are rotated 45° to define a face-centered square lattice of Ni ions. The lattice constants in these directions are then $\sqrt{2}$ times the Ni-Ni nearest-neighbor distance a in the basal plane. The lattice constant c remains the same as

---

TABLE I. Candidate symmetric μ^+ stopping sites in La$_4$Ni$_3$O$_8$. Coordinates are fractions of lattice parameters in the $I4/mmm$ and $F4/mmm$ settings (see text). Coordinates and O^{2-} distances from lattice data of Ref. [3].

| μ^+ site | $I4/mmm$ | | | Wycoff | $F4/mmm$ | | O^{2-} distance | |
	x	y	z^{a}	designation	x	y	(Å)	Location
$\mu1$	$\frac{1}{4}$	$\frac{1}{4}$	0	$8h$	0	$\frac{1}{4}$	1.4039	nn O in ab plane
$\mu2$	$\frac{1}{4}$	$\frac{1}{4}$	0.1256	$16m$	0	$\frac{1}{4}$	'' ''	'' ''
$\mu3$	$\frac{1}{4}$	$\frac{1}{4}$	$\frac{1}{4}$	$8f$	0	$\frac{1}{4}$	'' ''	'' ''
$\mu4$	0	$\frac{1}{2}$	0.1878	$8g$	$\frac{1}{4}$	$\frac{1}{4}$	1.6238	nn O along c axis
$\mu5$	0	$\frac{1}{2}$	0.0628	$8g$	$\frac{1}{4}$	$\frac{1}{4}$	1.6394	'' ''
$\mu6$	$\frac{1}{2}$	$\frac{1}{2}$	0	$2b$	0	$\frac{1}{2}$	1.9854	centered in O square
$\mu7$	$\frac{1}{2}$	$\frac{1}{2}$	0.1256	$4e$	0	$\frac{1}{2}$	'' ''	'' ''
$\mu8$	$\frac{1}{2}$	$\frac{1}{2}$	$\frac{1}{4}$	$4e$	0	$\frac{1}{2}$	'' ''	'' ''

in the $I4/mmm$ setting, and the unit-cell volume is doubled. The observed charge-stripe supercell [5] is $3\sqrt{2}a \times \sqrt{2}a \times c$, where the stripe direction is the b axis (cf. Fig. 1). Candidate μ^+ sites are given in Table I for both settings.

In the $I4/mmm$ tetragonal unit cell there are a total of 58 such sites (the sum of the Wycoff multiplicities in Table I). With two trilayers per $I4/mmm$ unit cell, there are 58 sites per trilayer in the $F4/mmm$ setting and $3 \times 58 = 174$ sites per trilayer in a stripe supercell. The two trilayers are crystallographically equivalent, so that it is sufficient to consider μ^+ sites for a single trilayer provided this equivalence extends to the ordered magnetic structure. Figure 3 shows two $F4/mmm$ supercells of La$_4$Ni$_3$O$_8$ viewed along the c axis, with the stripe AFM configuration of Fig. 1 [23] and μ^+ sites from Table I. The number of magnetically inequivalent sites in a full 3D AFM configuration is clearly greater in stripe models than for AFM order without stripes.

The μ^+ sites of Table I may not be realistic: they would be unstable if the O^{2-} ions were classical point charges, and our calculations do not take account of off-site ionic positions,
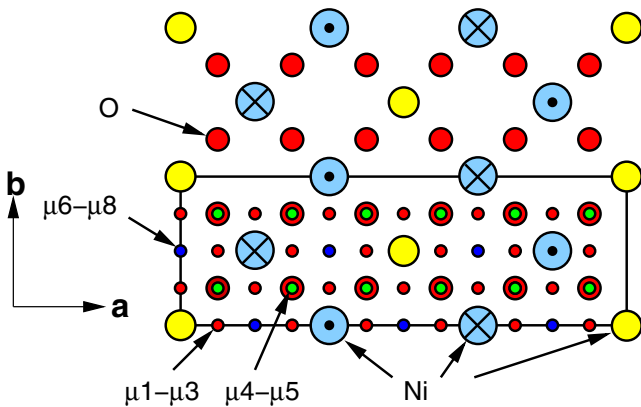
intrinsic to the La$_4$Ni$_3$O$_8$ crystal structure [23] or due to the μ^+ charge. The candidate sites sample a large fraction of the unit cell, however (Fig. 2), so that calculated dipolar fields at these sites in the magnetically ordered phase can be taken as rough guides to the local field distribution.

V. ANTIFERROMAGNETIC CONFIGURATIONS

A. Experimental results

Figure 4 shows Fourier transforms of ZF-μSR asymmetry data from La$_4$Ni$_3$O$_8$ from 2.2 to 110 K. There are at least six discrete peaks with nonzero frequency, corresponding to oscillations in the asymmetry spectra due to μ^+ spin precession in well-defined magnetic fields. The peaks are clearly visible at 50 K; we label them from 1 to 6 on the abscissa of Fig. 4. In the temperature range 99–105 K the frequency of peak 6 ($\sim$19 MHz) hardly changes, but its amplitude decreases smoothly to nearly zero. Several of the peaks are broad, and probably contain unresolved frequencies from multiple sites.

A representative series of ZF-μSR asymmetry spectra for temperatures between 1.85 and 105 K (the AFM phase) is shown in Fig. 5. The curves in Fig. 5 are fits to the data using the exponentially damped multifrequency function

$$G(t) = f_0 \exp(-\lambda_0 t) + \sum_{i=1}^{6} f_i \exp(-\lambda_i t) \cos(\omega_i t + \phi_i) \quad (1)$$

for the μ^+ spin polarization.[3] The frequencies ω_i give the local magnetic fields ω_i/γ_μ, where $\gamma_\mu = 8.5156 \times 10^4\,\mathrm{s^{-1}\,G^{-1}}$ is the gyromagnetic ratio of the muon. The rates λ_i characterize line broadening, dominated by inhomogeneity in these fields. The amplitudes f_i are related to μ^+ site occupation probabilities, and are not expected to depend on temperature. The polycrystalline nature of our sample is not involved in the ZF results shown in Fig. 5, except that the f_i are averaged over

FIG. 3. 2D AFM structure of Fig. 1 [23] and projections of candidate μ^+ stopping sites in La$_4$Ni$_3$O$_8$ (Fig. 2 and Table I) onto the ab plane in the $F4/mmm$ setting of the $3\sqrt{2}a \times \sqrt{2}a$ 2D stripe supercell. Large circles: blue: Ni^{1+} ($S = 1/2$) ($\odot$ = up spins; $\otimes$ = down spins); yellow: Ni^{2+} ($S = 0$); red: O^{2-}. Small circles: μ^+ sites from Table I. Rectangle: supercell boundary.

---

[3] For ZF measurements in a random powder with static local fields, $\frac{1}{3}$ of the initial μ^+ polarization relaxes with zero frequency [26]. A $\omega = 0$ component is also present in an antiferromagnet if a muon site is symmetric with respect to the sublattices since this results in cancellation of local fields.
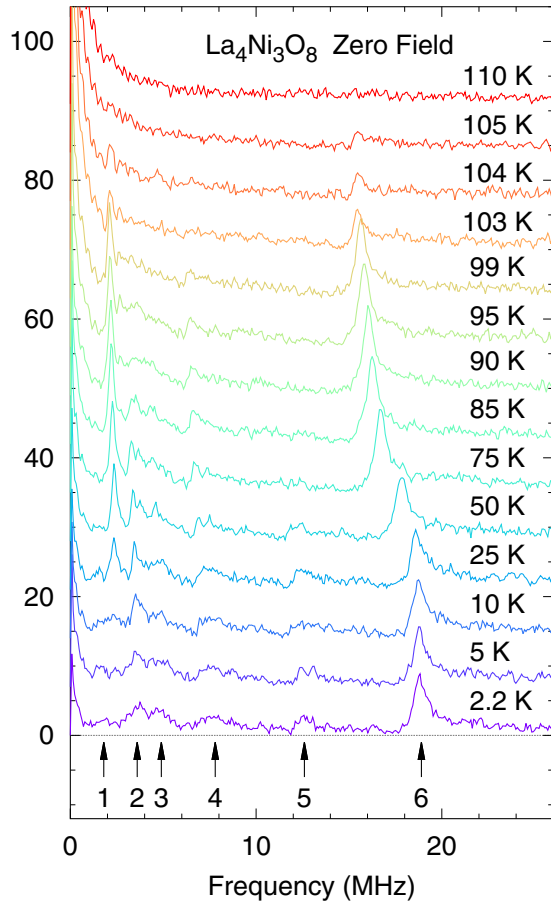
FIG. 4. Fourier-transform spectra from ZF-μSR asymmetry data (cf. Fig. 5) in La$_4$Ni$_3$O$_8$, 2.2 K $\leqslant T \leqslant$ 110 K. The spectra are offset for clarity. Arrows: discrete frequencies at 2.2 K.

local-field orientations relative to the initial μ^+ polarization direction.

Frequencies obtained from fits of Eq. (1) to asymmetry data are plotted vs temperature in Fig. 6(a) and similarly labeled from 1 to 6. The rather smooth differences in temperature dependence of the frequencies between T_N and $\sim$25 K is evidence for a gradual Ni spin reorientation below the transition.

The amplitudes and rates of peak 1 ($\sim$2 MHz) and peak 6 are compared in Figs. 6(b) and 6(c). They behave quite differently: below $\sim$90 K the amplitude and rate of peak 6 are nearly constant, whereas for peak 1 they both increase substantially with decreasing temperature below $\sim$25 K. At lower temperatures, peak 1 is hard to see in the Fourier spectra (Fig. 4) because its increase in time-domain (asymmetry) amplitude by a factor of $\sim$2 [Fig. 6(b)] (probably an artifact due to overlapping adjacent peaks) is offset[4] by a damping-rate (linewidth) increase by a factor of $\sim$30 [Fig. 6(c)]. This behavior is discussed in detail in Sec. VII A 2.

---

[4]Due to the general Fourier-transform proportionality between time-domain amplitudes and frequency-domain areas, increased broadening causes a loss of frequency-domain amplitude.
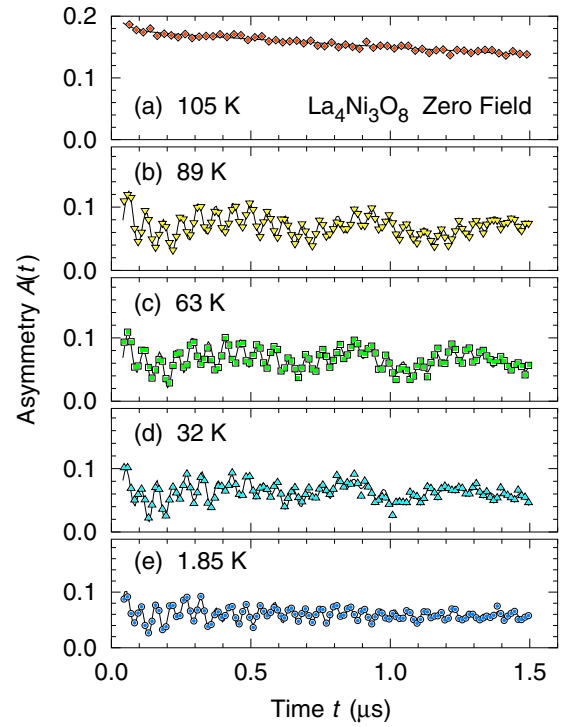

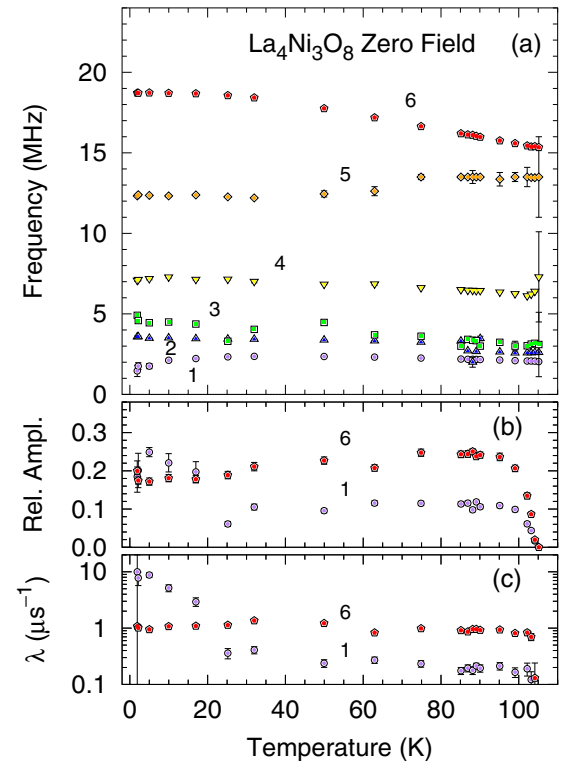FIG. 5. Representative ZF-μSR asymmetry spectra in La$_4$Ni$_3$O$_8$, $T \leqslant T_N = 105$ K. Curves: fits of Eq. (1) to the data.

FIG. 6. Temperature dependence of parameters in La$_4$Ni$_3$O$_8$ from fits of Eq. (1) to ZF-μSR asymmetry data (cf. Fig. 5). Numbers indicate peaks in Fig. 4. (a) μ^+ precession frequencies. (b) Relative oscillation amplitudes of peaks 1 and 6 (Fig. 4). (c) Exponential damping rates of peaks 1 and 6.
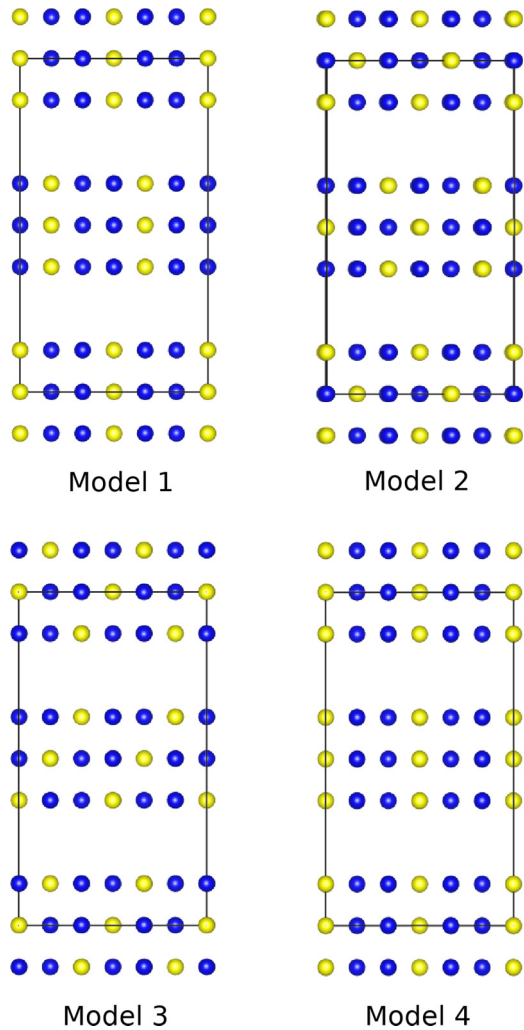
Model 1   Model 2

Model 3   Model 4

FIG. 7. Models for charge stripes in $La_4Ni_3O_8$. Numbering as in Ref. [5]. Blue spheres: Ni^{1+} ions ($S = \frac{1}{2}$); yellow spheres: Ni^{2+} ions ($S = 0$); rectangles: $3\sqrt{2}a \times \sqrt{2}a \times c$ supercell outlines. The view is along the stripe (*b*) direction.

B. Models of AFM order: Dipolar-field calculations

This section describes lattice-sum calculations of Ni-moment dipolar magnetic fields at the candidate μ^+ stopping sites of Table I for a number of candidate AFM configurations, with and without charge stripes. The calculations assume the same moment on all moment-bearing Ni^{1+} ions in a trilayer, consistent with the neutron diffraction results [6]. These dipolar fields are summed over a sphere of radius 200 Å centered on the μ^+ site, after determining that increasing this radius does not affect the results appreciably. The Ni-ion moment is scaled for rough agreement of the dipolar-field frequencies with a typical experimental spectrum ($T = 50$ K, cf. Fig. 4).

1. AFM configurations with charge stripes

a. Stripe models. For completeness, we consider the four charge-stripe models discussed by Zhang *et al.* [5], which differ in the positions of the stripes on the individual layers. These models are shown in Fig. 7, where the view is along the stripe direction (the *b* direction in the $F4/mmm$ setting), and a supercell boundary is shown. The model numbering (1–4) of Ref. [5] is used in the following. The stripes in a trilayer are stacked along the *c* axis in models 1 and 4 and staggered in models 2 and 3. The Coulomb repulsion energy would seem to be lower for the latter, but x-ray diffraction data favor the stripe structure of model 1 [5]. The latter is also used for AFM configurations in the neutron diffraction study of Ref. [6]. Model 4 is assumed in the *ab initio* treatment of charge and AFM order in $La_4Ni_3O_8$ of Botana *et al.* [23], where it is argued that the weak coupling between trilayers does not play a significant role in the electronic structure.

The calculations and neutron diffraction results cited above [6,23] both yield the 2D AFM structure shown in Fig. 1, with Ni moments aligned along the *c* axis. We have calculated dipolar fields at μ^+ sites for 16 3D AFM structures, obtained by placing 2D AFM layers with this structure on each of the four stripe models in four configurations, designated A–D in the following. In configuration A the moment orientations are those of Fig. 1 on all layers. In configuration B all moments on alternate trilayers of configuration A are inverted. In configuration C the Ni2 (middle layer) moments of configuration A are inverted for all layers, yielding intratrilayer AFM ordering. Configuration D can be obtained in either of two ways: by inverting the Ni2 moments of configuration B, or by inverting alternate trilayers of configuration C.

We discuss model 1 below. Models 2–4 are described in Appendix A.

b. Dipolar fields in stripe model 1. The four AFM moment configurations are shown in Fig. 8 for charge-stripe model 1, and histograms of frequencies from μ^+-site dipolar-field calculations for these configurations are compared with the observed 50-K spectrum in Fig. 9. The calculated histograms assume equal stopping probabilities for all μ^+ sites, which may not be the case, and do not take into account possible transferred μ^+ hyperfine fields. A rough correspondence between the calculated histograms and observed spectra is obtained with Ni^{1+} moments 0.4–0.5 μ_B, somewhat smaller than the predicted values 0.6–0.7 μ_B [23]. A high-frequency group of peaks is separated from a low-frequency group by a region with less spectral weight. The comparison suggests that the high-frequency peak is formed from a group of discrete frequencies. These are mainly from μ1 sites, which is not surprising as they are the closest to Ni ions (Fig. 3).

There are a number of general features of the calculated histograms (Fig. 9 and Appendix A). Histograms for stripe models 1 and 4 are similar, as are those for stripe models 2 and 3, due to stacked stripes in the former compared to offset stripes in the latter. For a given model, only small differences and no change of Ni moment are found between A and B histograms, and also between C and D histograms. Inverting alternate trilayers changes the μ^+-site fields considerably less than inverting Ni2 moments within each trilayer.

Reference [6] concludes that trilayers are essentially uncorrelated along the *c* axis, corresponding to a random mix of configurations 1A and 1B (or 1C and 1D). From Fig. 9, such a random mix would have little effect on the higher frequencies, which arise from μ^+ sites in or near the trilayers. There are visible changes of the lower frequencies associated with sites
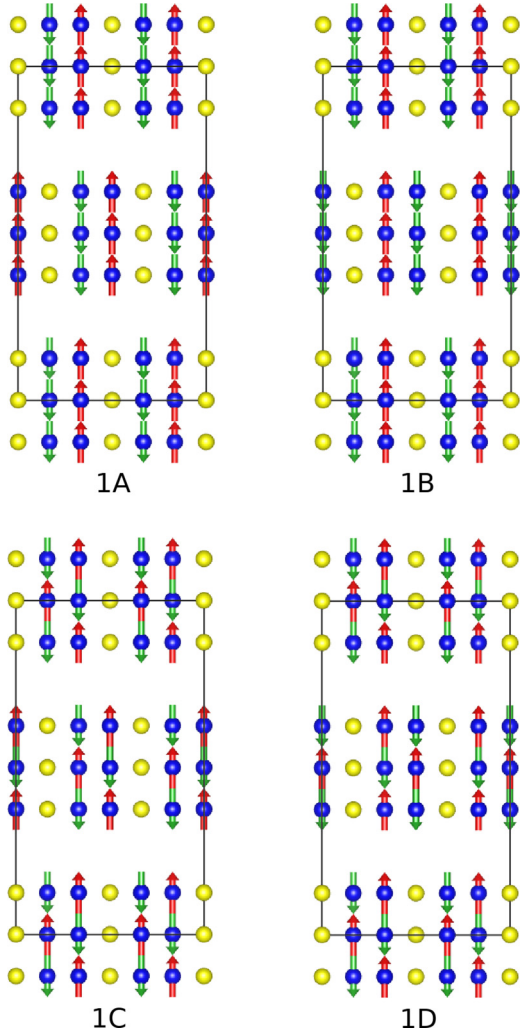
FIG. 8. AFM moment configurations A–D in $La_4Ni_3O_8$ on charge-stripe model 1 [5]. Blue spheres: Ni^{1+} ions ($S = \frac{1}{2}$); yellow spheres: Ni^{2+} ions ($S = 0$); rectangles: $3\sqrt{2}a \times \sqrt{2}a \times c$ supercell outlines; arrows: AFM ordered moments. The view is along the stripe (b) direction.

far from trilayers. This behavior may have been observed, as described below in Sec. VII A 2.

For all stripe models a calculated peak or group is found near the observed small peak at ∼12 MHz for AFM configurations A and B but not for configurations C and D; agreement with the observed spectrum is better for the former configurations. This is not strong evidence for them, however, due to the approximate nature of the treatment and the uncertainty in the μ^+ sites. Nevertheless, we note the discrepancy between this result and the neutron scattering data [6], which favor the AFM intratrilayer order of configurations 1C and 1D (trilayer model 5 of Ref. [5], Supplemental Material) over the FM intratrilayer order of configurations 1A and 1B (their model 6).

2. AFM order without stripes?

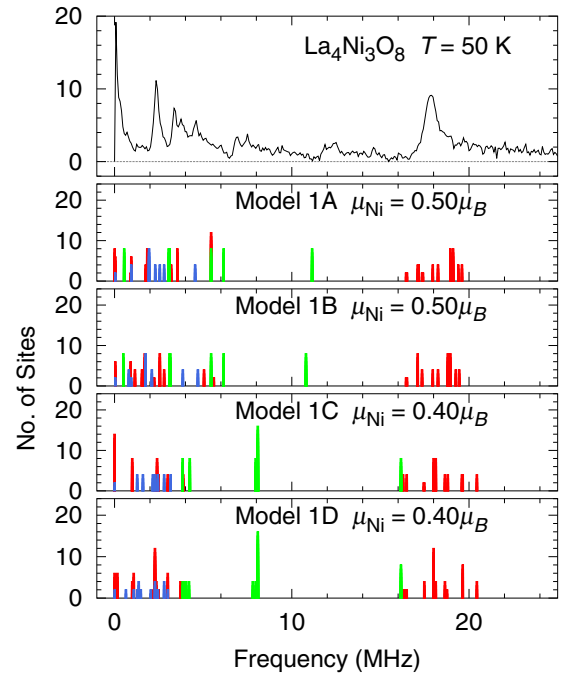For completeness we also consider AFM configurations without stripes (although these are ruled out by the neutron

FIG. 9. Histograms of dipolar-field μ^+ frequencies from AFM stripe models 1A–1D compared to 50-K μSR FT spectrum in $La_4Ni_3O_8$, $T = 50$ K. Colors indicate μ^+ site groups (Table I): red: $\mu1–\mu3$; green: $\mu4–\mu5$; blue: $\mu6–\mu8$.

diffraction results [6]). Using the $F4/mmm$ setting, Fig. 10 shows four such configurations in $La_4Ni_3O_8$: the ferromagnetic (FM) configuration (for completeness), and three AFM configurations [16,18–20]. Figure 11 compares frequency histograms from dipolar field calculations for the configurations of Fig. 10 with the observed 50-K spectrum. The subscripts 1 and 2 for the FM and A-AFM configurations designate alternate trilayer moments as pictured in Fig. 10 or inverted, respectively. Alternate-trilayer inversion followed by 90° rotation about the c axis is a symmetry operation for the C-AFM and G-AFM configurations, and therefore does not affect the dipolar-field histogram.

These histograms have a rough correspondence with those for the stripe-model AFM configurations of the previous section and, similarly, have no clear agreement with details of the experimental spectrum. This is not surprising since commensurate stripes are long-range order (i.e., points in reciprocal space) best probed by a diffraction technique, whereas μSR, like NMR, is a point probe in real space. The histograms of Fig. 11 are not as dense as those from stripe configurations, and there does not seem to be enough spectral weight at low frequencies, but the evidence for a striped AFM configuration from neutron diffraction [6] is much more compelling.

VI. PARAMAGNETIC PHASE

Two mechanisms for μ^+ spin relaxation are expected in the high-temperature paramagnetic phase of a local-moment magnet: dynamic relaxation due to local-moment fluctuations, and (quasi)static relaxation from nuclear dipolar fields. In zero or low applied fields the resulting Kubo-Toyabe (KT) relaxation [26] is due to the combined effects of these mechanisms.
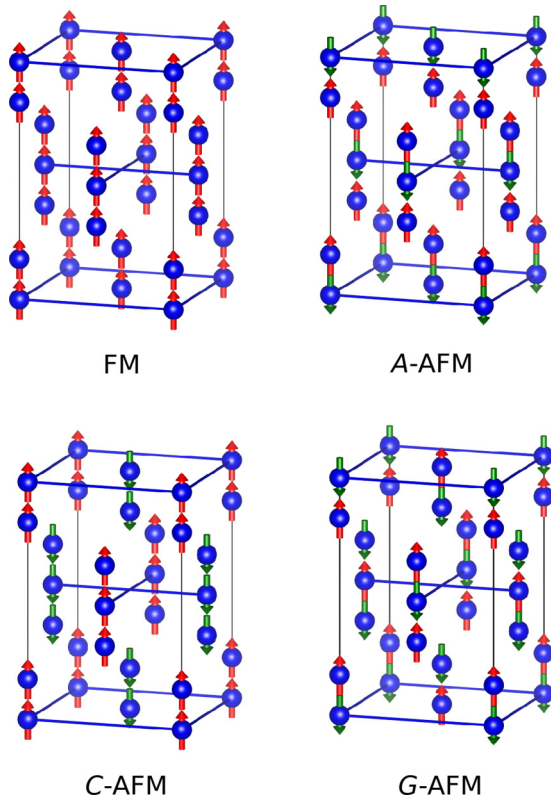
FIG. 10. AFM Ni-ion moment configurations without stripes in La$_4$Ni$_3$O$_8$, $F4/mmm$ setting. *A*-AFM: FM intratrilayer, AFM intertrilayer. *C*-AFM: AFM intratrilayer, FM intertrilayer. *G*-AFM: AFM intratrilayer, AFM intertrilayer.

LF-μSR is a standard method for separation of the static and dynamic contributions [8] since a longitudinal field H_L "decouples" the μ^+ spin polarization from the static local field distribution.[5] Static μ^+ relaxation functions $G_s(H_L, t)$ for arbitrary H_L (including zero field) have been determined for several local field distributions [8,26–28]. The combined effect of static and dynamic relaxation is often modeled by exponential damping of $G_s(H_L, t)$ with rate λ:

$$G(H_L, t) = e^{-\lambda t} G_s(H_L, t). \quad (2)$$

In La$_4$Ni$_3$O$_8$, $G(H_L, t)$ is complicated by the large number of inequivalent μ^+ sites. This results in a broad inhomogeneous distribution of μ^+ dipolar fields from Ni^{1+} moments, as can be seen from the AFM-phase histograms discussed above. Similarly, the dipolar-field distribution from randomly oriented ^{139}La nuclei is further broadened because of the multiple μ^+ sites. Obtaining $G(H_L, t)$ is then a difficult numerical problem even if these distributions were known, which is not the case for La$_4$Ni$_3$O$_8$ because of uncertainty in the μ^+ sites.

We have carried out ZF- and LF-μSR experiments in the paramagnetic phase of La$_4$Ni$_3$O$_8$ between T_N and 275 K. For

---

[5]For large enough H_L ($\gg$ the local-field distribution width) the resultant field is parallel to the μ^+ spin polarization. Then there is no precession and thus no static relaxation, so that any observed relaxation is dynamic.
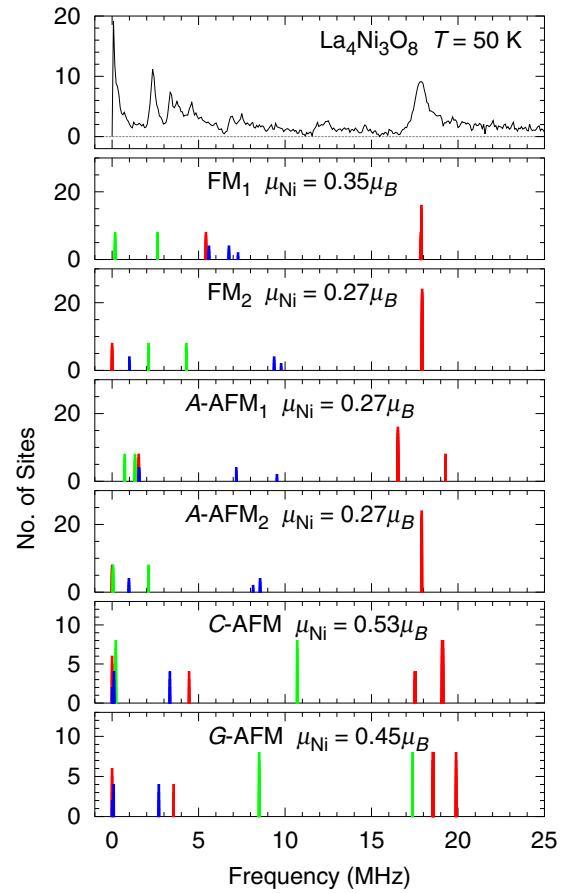

FIG. 11. Histograms of dipolar-field μ^+ frequencies from AFM configurations without stripes (Fig. 10) compared to 50-K μSR FT spectrum in La$_4$Ni$_3$O$_8$. See text for notation. Colors as in Fig. 9.

analysis of the data we have chosen a rough approximate form of Eq. (2), using the static Lorentzian KT function $G_s^{\mathrm{Lor}}(H_L, \alpha, t)$ [27] with "stretched exponential" damping:

$$G(H_L, \alpha, t) = \exp[-(\lambda^* t)^K] G_s^{\mathrm{Lor}}(H_L, \alpha, t). \quad (3)$$

We have taken a Lorentzian distribution of ^{139}La dipolar fields with half-width α/γ_μ as an approximation beyond the Gaussian that is appropriate for a single μ^+ site in a homogeneous system [26]. The LF static Lorentzian KT function is [27]

$$
\begin{aligned}
G_s^{\mathrm{Lor}} = \ &1 - \frac{\alpha}{\omega_L} j_1(\omega_L) \exp(-\alpha t) \\
&- \left(\frac{\alpha}{\omega_L}\right)^2 [j_0(\omega_L t) \exp(-\alpha t) - 1] \\
&- \alpha \left[1 + \left(\frac{\alpha}{\omega_L}\right)^2\right] \int_0^t j_0(\omega_L \tau) \exp(-\alpha \tau) \, d\tau, \quad (4)
\end{aligned}
$$

where $\omega_L = \gamma_\mu H_L$, and j_0 and j_1 are spherical Bessel functions. In the ZF limit Eq. (4) simplifies to

$$G_s^{\mathrm{Lor}}(\alpha, t) = \tfrac{1}{3} + \tfrac{2}{3}(1 - \alpha t) \exp(-\alpha t). \quad (5)$$

The stretched-exponential form of the damping in Eq. (3) represents an inhomogeneous distribution of local dynamic
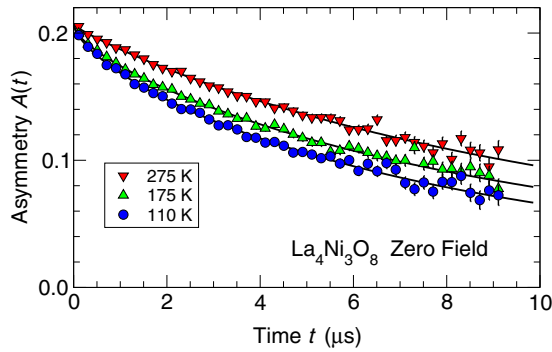
FIG. 12. Representative zero-field μSR asymmetry relaxation in La$_4$Ni$_3$O$_8$, $T > T_N$. Legend: temperature values. Curves: fits of Eqs. (3) and (5) to the data.

FIG. 14. Representative longitudinal-field μSR asymmetry relaxation in La$_4$Ni$_3$O$_8$, $T = 200$ K. Legend: values of the longitudinal field H_L. Curves: fits of Eqs. (3) and (4) to the data.

relaxation rates λ_{loc} [29,30], where λ^* is a characteristic rate (but not the average [30]) and the stretching power $K < 1$ characterizes the distribution function $P(\lambda_{\text{loc}})$ of the local rates.

The stretched-exponential dynamic and Lorentzian static forms are crude approximations (both are strictly valid only for a r^{-3} interaction with local moments in the dilute limit [27,31]). Their use is justified by their relative simplicity, and *a posteriori* by the fact that they give good fits to the data (see below). An alternative model for static relaxation in disordered systems, the "Gaussian broadened Gaussian" KT function [28], does not fit well; for early times it varies as t^2 (i.e., as a Gaussian), whereas the data exhibit the linear early-time behavior of an exponential [27].

A. Zero field

Representative ZF asymmetry spectra above T_N are shown in Fig. 12, and Fig. 13 shows the temperature dependence of λ^* and K in zero field from fits of Eqs. (3) and (5) to the data. In the fits α was fixed at its 200-K value, but the results do not

change qualitatively for $\pm 10\%$ variations of α. The stretching power $K(T)$ is essentially constant, whereas $\lambda^*(T)$ increases markedly with decreasing temperature as T_N is approached.

The curves in Fig. 13(a) give fits of theoretical expectations for 2D AFM spin fluctuations [10,32,33], as discussed in Ref. [12] with respect to ^{139}La NMR relaxation data. The solid curve is a phenomenological Curie-Weiss–type fit: $\lambda^*(T) \propto T/(T - T_0)$ [32,33], which yields $T_0 = 90(1)$ K. The dashed curve in Fig. 13(a) is the function

$$\lambda^*(T) \propto x^{3/2} e^{1/x}/(1+x)^3, \quad x = T/1.13J \qquad (6)$$

derived by Chakravarty and Orbach [10] (CO) from the theory of a 2D quantum Heisenberg antiferromagnet [9] mentioned in Sec. II, in which the critical point is at $T = 0$. The weak interlayer interaction that precipitates the 3D AFM transition in this picture is not expected to affect the critical behavior appreciably. Equation (6) is only valid for $T < 0.57J$, however [10], where J is the AFM exchange coupling. The fit value of J is 86(22) K, so that temperatures in the paramagnetic phase of La$_4$Ni$_3$O$_8$ violate this condition. Thus, the CO fit is inconsistent.

B. Longitudinal field, $T = 200$ K

Figure 14 shows representative asymmetry spectra at 200 K for $0 \leqslant H_L \leqslant 4$ kOe. The curves are fits of Eqs. (3) and (4) to the data. The observed spectra are quite smooth, and the parameters α, λ^*, and K in Eqs. (3)–(5) are highly correlated statistically, making it hard to determine them separately. The following procedure was used: at high enough fields $G_s^{\text{Lor}}(H_L, t) = 1$ independent of α, so that stretched-exponential fits determine λ^* and K. Assuming these are roughly field independent, they were fixed and the lowest-field data were fit to determine α. Then all three parameters were iteratively fixed and freed at low fields: α was fixed and λ^* and K freed, and vice versa, until convergence was obtained. Finally α was fixed, and λ^* and K were freed for fits at all fields.

For low fields, the overall relaxation slows with increasing field but the early-time relaxation is not affected, which is a characteristic of static local-field decoupling. For higher fields the initial slope decreases, indicating a field dependence of λ^* and/or K.

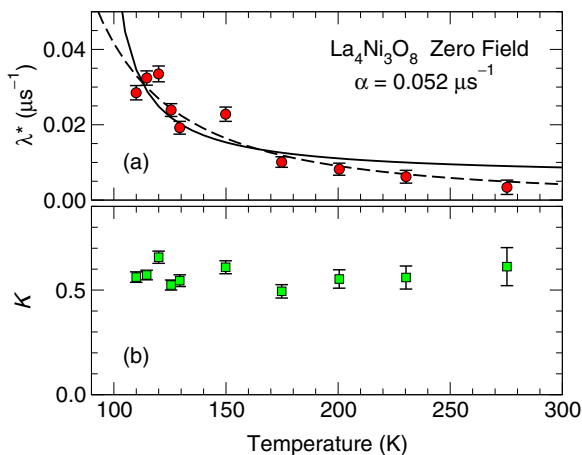FIG. 13. Temperature dependence of zero-field dynamic relaxation parameters in La$_4$Ni$_3$O$_8$, $T > T_N$. (a) Stretched-exponential relaxation rate λ^*. Solid curve: fit of $\lambda^*(T) \propto T/(T - T_0)$ [32,33] to the data, $T_0 = 90(1)$ K. Dashed curve: fit of Eq. (6) from the CO theory [10] to the data, $J = 86(22)$ K. (b) Stretching power K.
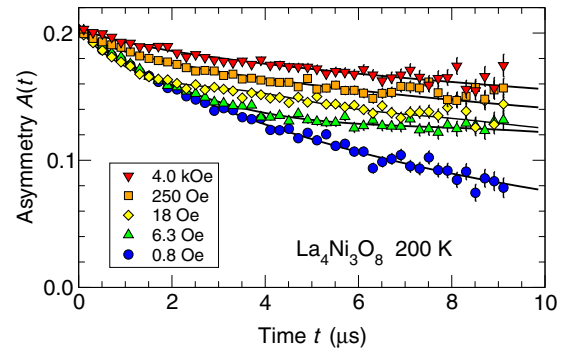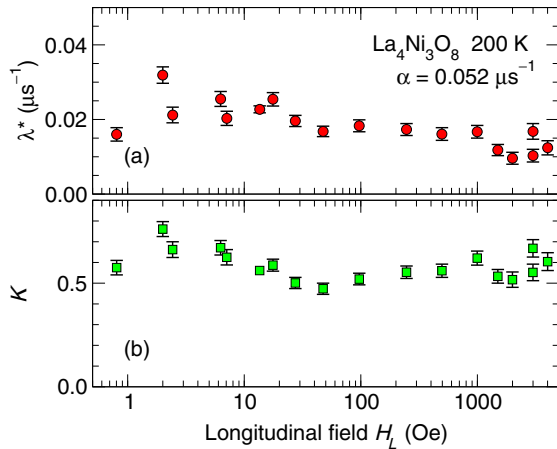
FIG. 15. Field dependence of longitudinal-field dynamic relaxation parameters in $La_4Ni_3O_8$, $T = 200$ K. (a) Stretched-exponential relaxation rate λ^*. (b) Stretching power K.

FIG. 17. Field dependence of longitudinal-field dynamic relaxation parameters in $La_4Ni_3O_8$, $T = 110$ K. (a) Stretched-exponential relaxation rate λ^*. (b) Stretching power K.

The field dependencies of λ^* and K at 200 K are shown in Fig. 15. The scatter in the parameters is obviously strongly correlated. The field dependencies at low fields are probably artifacts of the assumed field independence of α; a field dependence (as discussed in Ref. [26] for the Gaussian relaxation rate at a single μ^+ site) might be expected in $La_4Ni_3O_8$ because the μ^+ frequency $\gamma_\mu H_L$ is of the order of the lower of the two observed ^{139}La quadrupolar splittings [4] for $H_L \sim 100$ Oe. Nevertheless, for $H_L \gtrsim 50$ Oe the fits no longer depend on α, and the parameters are only weakly field dependent. The stretching power K is close to the value $\frac{1}{2}$ expected from a Lorentzian distribution of fluctuating fields in the motional-narrowing limit (rapid fluctuations) [27,31], which is perhaps further justification for the use of Lorentzian distributions to describe μ^+ relaxation in $La_4Ni_3O_8$.

C. Longitudinal field, $T = 110$ K

A similar analysis was applied to LF data taken for $T = 110$ K, a temperature just above T_N. Representative asymmetry spectra are shown in Fig. 16, and the field dependencies of λ^* and K, determined as described above for 200 K, are shown in Fig. 17. The values of K at the two temperatures are
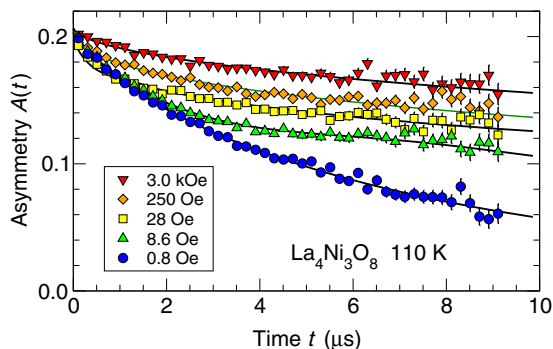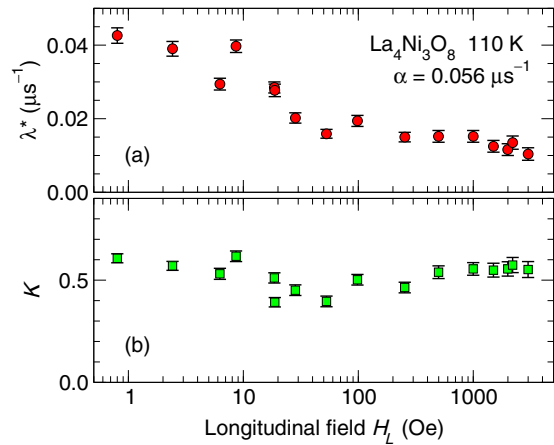

FIG. 16. Representative longitudinal-field μSR asymmetry relaxation in $La_4Ni_3O_8$, $T = 110$ K. Legend: values of the longitudinal field H_L. Curves: fits of Eqs. (3) and (4) to the data.

comparable, but at 110 K a clear increase of λ^* at low fields is observed. This increase and the temperature independence of λ^* at high fields are discussed further in Sec. VII B.

Values of λ^* for $H_L = 0.8$ Oe at $T = 200$ and 110 K (Figs. 15 and 17) are larger than the ZF values at those temperatures (Fig. 13). This field dependence at low fields is not presently understood.

VII. DISCUSSION

A. AFM transition and spin configuration

The complex zero-field μSR spectra observed below 105 K in $La_4Ni_3O_8$ (Fig. 4) clearly indicate the magnetic nature of the transition. The multiple frequencies arise from a number of magnetically inequivalent μ^+ stopping sites in the crystal. The sharp peaks indicate commensurate magnetic order since in an incommensurate structure crystallographically equivalent μ^+ stopping sites would be subject to a continuous distribution of frequencies. The smooth differences in temperature dependencies of the various peak frequencies between T_N and $\sim$25 K [Fig. 6(a)] suggest reorientation of the AFM magnetic structure with decreasing temperature below T_N.

1. Abrupt onset at T_N

From Figs. 4–6 we conclude that the transition at $T_N = 105$ K has an abrupt onset since the peak frequencies appear discontinuously at T_N. This is suggestive of a first-order transition. It is, however, also consistent with a continuous second-order transition in an inhomogeneous system [34], if the intrinsic onset of the order parameter is sufficiently abrupt (i.e., the critical exponent β is sufficiently small) compared to the width of the inhomogeneous transition temperature distribution. A simple model for zero-field μSR (and NQR) spectra in this situation, described in Appendix B, shows that near T_N the spectra become broadly distributed, with reduced-amplitude peaks at their maxima. Then the transition appears discontinuous (Fig. 25), as we observe in $La_4Ni_3O_8$ (Fig. 4). We cannot discriminate between this and a true first-order

discontinuity on the basis of our data (the term "abrupt" describes both possibilities).

a. Comparison with neutron diffraction. A commensurate AFM phase is found in $La_4Ni_3O_8$ by neutron Bragg diffraction [6], but with a smooth continuous transition. This discrepancy with the μSR result can be understood in the above scenario [34,35]. The effect of the distribution is quite different in the two techniques, due to the fact that magnetic resonance experiments probe real space whereas neutron diffraction probes reciprocal space. In neutron diffraction the AFM Bragg intensity is proportional to the volume fraction of magnetic order, and therefore increases smoothly as the temperature is decreased through an inhomogeneous distribution of transition temperatures.

b. Comparison with NMR. The μSR evidence for an abrupt transition in $La_4Ni_3O_8$ is also in conflict with the smooth transition observed in ^{139}La NMR spectra [Ref. [4] (supplement)]. The NMR spectra were obtained from a partially oriented powder sample in an applied field of 42 kOe rather than zero field, and the conclusion of a smooth transition is mainly based on a single point at $\sim$95 K. It seems possible that partial random orientation and/or the applied field affected the results in these experiments.

c. Comparison with other materials. μSR studies of the doped nickelate $La_{2-x}Sr_xNiO_4$ [36–38] yield an abrupt but continuous frequency onset at T_N with a small value of the critical exponent β, similar to our results in $La_4Ni_3O_8$.

Discontinuous transitions were observed in the layered AFM cuprate $La_2CuO_{4+\delta}$ in ^{139}La NQR [39] and other hyperfine experiments [40,41], but not in neutron diffraction; the discrepancy can be understood as noted above in Sec. VII A 1 a. Subsequent ^{139}La NQR experiments in a sufficiently homogeneous $La_2CuO_{4+\delta}$ crystal [34] resolved an "abrupt but continuous" change of frequency at the transition. Our results in $La_4Ni_3O_8$ might also be due to such an inhomogeneity-induced discontinuity, and there is a clear need for experiments on more homogeneous samples of this compound.

2. AFM spin configuration

Histograms of calculated Ni-ion dipolar fields at candidate μ^+ sites for a number of charge-stripe models and AFM configurations (Sec. V B, Appendix A) capture the general features of frequency spectra and suggest reduced Ni moments (0.4–$0.5\mu_B$), but do not uniquely determine the specific AFM configuration. Dipolar-field histograms for AFM configurations without stripes have somewhat less structure than the observed spectra.

The broadening of peak 1 below $\sim$25 K [Fig. 6(d)] is evidence for the onset of significant disorder at low temperatures. The low-frequency peaks arise from μ^+ sites far from Ni trilayers, suggesting that the disorder is associated with the lack of c-axis correlation reported in Ref. [6]. The absence of broadening for peak 6, which is from μ^+ sites in or near the Ni trilayers, shows that the AFM state there is commensurate and not strongly disordered at low temperatures. Peak 1 becomes narrow above 25 K (Fig. 4), which indicates motional averaging of the corresponding local field.

This behavior suggests that the 105-K transition is within the trilayers and not between them. We speculate that at intermediate temperatures, each trilayer fluctuates dynamically as a whole but independently of neighboring trilayers, maintaining nearby μ^+ local fields more or less constant. Such "stripe fluctuation" has been reported in $La_{2-x}Sr_xNiO_4$ [38]. Below 25 K a weaker (possibly anisotropic) intertrilayer interaction leads to disordered full 3D spin freezing, with a broad distribution of local fields at μ^+ sites distant from trilayers.

B. Paramagnetic-phase relaxation; critical slowing

As discussed in Sec. VI A, increase of the ZF μ^+ relaxation rate $\lambda^*(T)$ as $T \to T_N$ from the paramagnetic phase [Fig. 13(a)] suggests critical slowing of spin fluctuations associated with the transition. The data can be fit with Eq. (6) from the CO theory [10], in which the critical fluctuations are 2D in nature and diverge as $T \to 0$. The value of the exchange constant J from this fit is lower than the temperatures of measurement, however, which invalidates the fit. A Curie-Weiss–type fit yields a divergence at 90(1) K, suggesting that it is associated with T_N rather than zero temperature.

Curie-Weiss and CO-theory fits [Fig. 13(a)] both yield characteristic temperatures (T_0 and J, respectively) of the order of T_N. This seems compatible with a connection between critical slowing and the 3D phase transition, although, as noted above, the CO fit is not valid.

Comparison of the field dependencies of $\lambda^*(T)$ at 200 K [Fig. 15(a)] and 110 K [Fig. 17(a)] suggests that the critical point is at zero field. The high-field data at both temperatures have similar magnitudes, but the low-field relaxation increases strongly with decreasing field at the lower temperature (which is close to T_N).

a. Comparison with NMR. Like the μSR data, the paramagnetic-phase ^{139}La nuclear spin-lattice relaxation rate in $La_4Ni_3O_8$ [12] can be fit with a Curie-Weiss law, but with a divergence as $T \to 0$ that disagrees strongly with the μSR result. The NMR data were also fit by Eq. (6), which was taken as evidence for the CO theory as discussed above. However, the exchange constant 129(5) K from the NMR data is, like that from the μSR data, of the order of T_N, and therefore the temperatures of measurement ($T > T_N$) do not obey the condition $T < 0.69J$ required for self-consistency of the theory [10]. Furthermore, the NMR experiments were carried out in a field of 42 kOe on very broad lines, which make the measurement difficult. For nonzero but much lower fields (0.1–4 kOe, Figs. 15 and 17) μ^+ spin relaxation rates show no sign of critical slowing between 200 and 110 K as noted above.

b. Specific heat peak. A peak in the temperature dependence of the specific heat is observed at T_N [4,5]. We note that a specific-heat "peak" could also be due to first-order latent heat in an inhomogeneous sample with a spread of transition temperatures. Furthermore, charge ordering in $La_4Ni_3O_8$ might contribute to the specific heat (μSR is not directly sensitive to charge ordering). Nevertheless, the peak has been taken as evidence for a second-order transition [12], which is not in conflict with the μSR relaxation data.
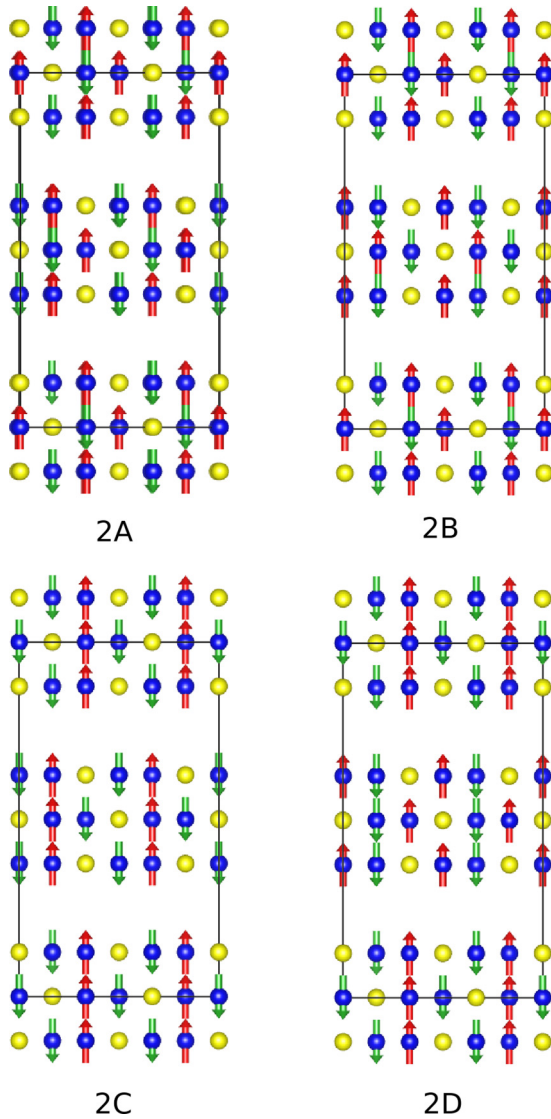
FIG. 18. AFM moment configurations A–D in La$_4$Ni$_3$O$_8$ on stripe model 2 [5]. See Fig. 8 for designations.

FIG. 19. Histograms of dipolar-field μ^+ frequencies from AFM stripe models 2A–2D compared to 50-K μSR FT spectrum in La$_4$Ni$_3$O$_8$. Colors as in Fig. 9.

c. Comparison with other materials. Critical slowing with a $T \to 0$ divergence was observed in NQR experiments on La$_2$CuO$_{4+\delta}$ [11], and taken as evidence for the CO theory [10]. Fits of Eq. (6) to the NQR data yield $T \ll J$ [11], consistent with applicability of the theory.

La$_4$Ni$_3$O$_8$ is intrinsically overdoped, and a more appropriate comparison might be with results from doped La$_2$CuO$_4$ with charge ordering. Previous ^{63,65}Cu and ^{139}La NQR studies of underdoped La$_{2-x}$Sr$_x$CuO$_4$, $0 \leqslant x \leqslant 0.15$ [11], found that critical slowing for $x = 0$ at high temperatures is rapidly suppressed by Sr doping. Recent NMR experiments [42,43] using a single crystal of La$_{1.885}$Sr$_{0.115}$CuO$_4$ revealed inhomogeneity and considerable structure associated with staging and oxygen diffusion at low temperatures, but did not revise the earlier conclusions. A NMR study [44] of single-crystal La$_2$CuO$_{4+y}$, $y \sim 0.11$, showed Curie-Weiss behavior of the ^{63}Cu relaxation rate for temperatures $\gtrsim 60$ K. This result is similar to both
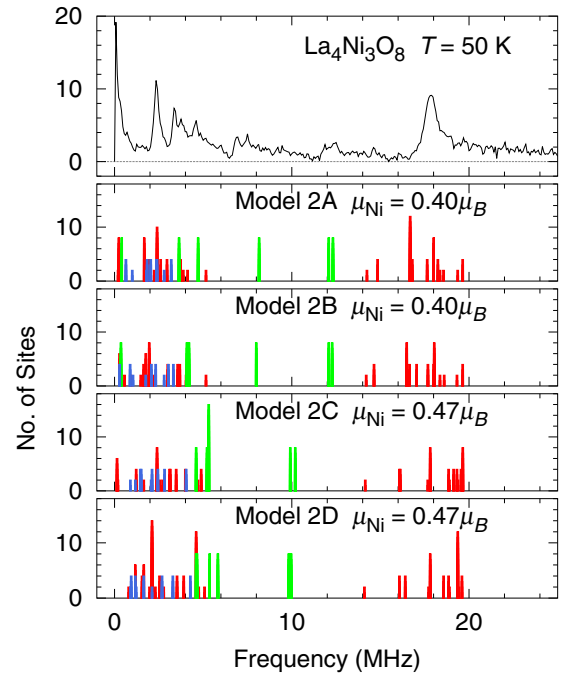
NMR and ZF-μSR data from La$_4$Ni$_3$O$_8$, but the doping level is higher in the nickelate. To our knowledge, no μSR studies of critical slowing in the paramagnetic phases of La$_2$CuO$_4$-based systems, doped or undoped, have been reported.

VIII. CONCLUSIONS

Comparison of μSR spectra in the AFM phase of La$_4$Ni$_3$O$_8$ with calculations of dipolar fields at candidate μ^+ sites does not determine the AFM configuration uniquely, but is consistent with the stripe structure from neutron diffraction and suggests a reduced ordered Ni^{1+} moment 0.4–0.5μ_B.

The nature of the 105-K transition is not well determined. Critical slowing is not expected for a first-order transition, however, and its observation is probably the best evidence that the transition in La$_4$Ni$_3$O$_8$ is "abrupt but continuous" [34].

The behavior of peaks 1 and 6 in the AFM spectra (Figs. 4 and 6) is strong evidence for commensurate AFM trilayers that fluctuate dynamically at temperatures between 25 K and T_N, and freeze with uncorrelated c-axis disorder below $\sim$25 K.

There is no evidence for 2D critical slowing with a divergence as $T \to 0$ in μSR data from La$_4$Ni$_3$O$_8$. The low-frequency spin dynamics of La$_4$Ni$_3$O$_8$ and La$_2$CuO$_{4+\delta}$ are not comparable, in spite of some similarities.

More work, both theoretical and experimental, is clearly necessary to understand the phase diagram of this enigmatic material.
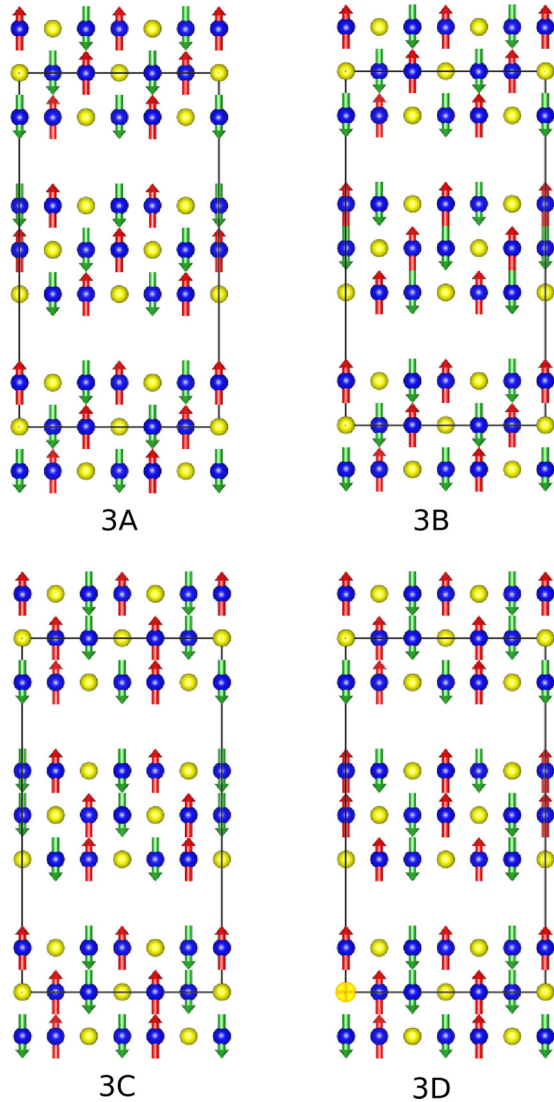
FIG. 20. AFM moment configurations A–D in $La_4Ni_3O_8$ on stripe model 3 [5]. See Fig. 8 for designations.

FIG. 21. Histograms of dipolar-field μ^+ frequencies from AFM stripe models 3A–3D compared to 50-K μSR FT spectrum in $La_4Ni_3O_8$. Colors as in Fig. 9.

APPENDIX A: OTHER AFM STRIPE MODELS

AFM configurations and corresponding dipolar-field histograms for stripe models 2–4 are shown in Figs. 18–23. The trends seen in model-1 histograms and discussed in Sec. V B 1 (low Ni moments, low- and high-frequency groups, only small changes for inverted alternate trilayers) continue to be found.
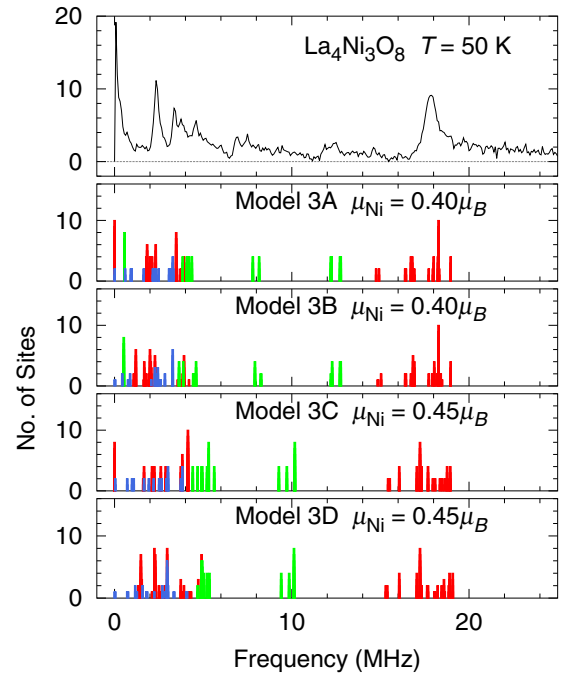
APPENDIX B: INHOMOGENEITY AND THE SPONTANEOUS FREQUENCY DISTRIBUTION FOR ABRUPT TRANSITIONS

We consider a simple model for a system with an abrupt second-order magnetic transition, i.e., a small value of the order-parameter critical exponent β. A first-order transition can be simulated by letting $\beta \to 0$.

The temperature dependence of a spontaneous zero-field frequency f (proportional to the order parameter) is assumed to be of the critical-exponent form

$$f(T, T_c) = f_0(1 - T/T_c)^\beta, \quad 0 < T < T_c \quad (B1)$$

where f_0 is the zero-temperature value. At a temperature T the frequency distribution function $P(f, T)$ (the spectrum) is given by

$$P(f, T) = \begin{cases} P[T_c(f, T)] \dfrac{dT_c(f, T)}{df}, & f_{\min} < f < f_{\max} \\ 0 \text{ otherwise}, \end{cases}$$
$$(B2)$$

where from Eq. (B1)

$$T_c(f, T) = \frac{T}{1 - (f/f_0)^{1/\beta}}, \quad (B3)$$

and $P(T_c)$ is the inhomogeneous distribution of transition temperatures T_c, taken to be nonzero for $T_c^{\min} < T_c < T_c^{\max}$. At a given temperature T, $P(f, T)$ lies between the limits $f_{\min(\max)}(T) = f(T, T_c^{\min(\max)})$. This yields

$$P(f, T) = \begin{cases} \dfrac{P[T_c(f, T)] \, T (f/f_0)^{1/\beta}}{\beta f [1 - (f/f_0)^{1/\beta}]^2}, & f_{\min} < f < f_{\max} \\ 0 \text{ otherwise}. \end{cases}$$
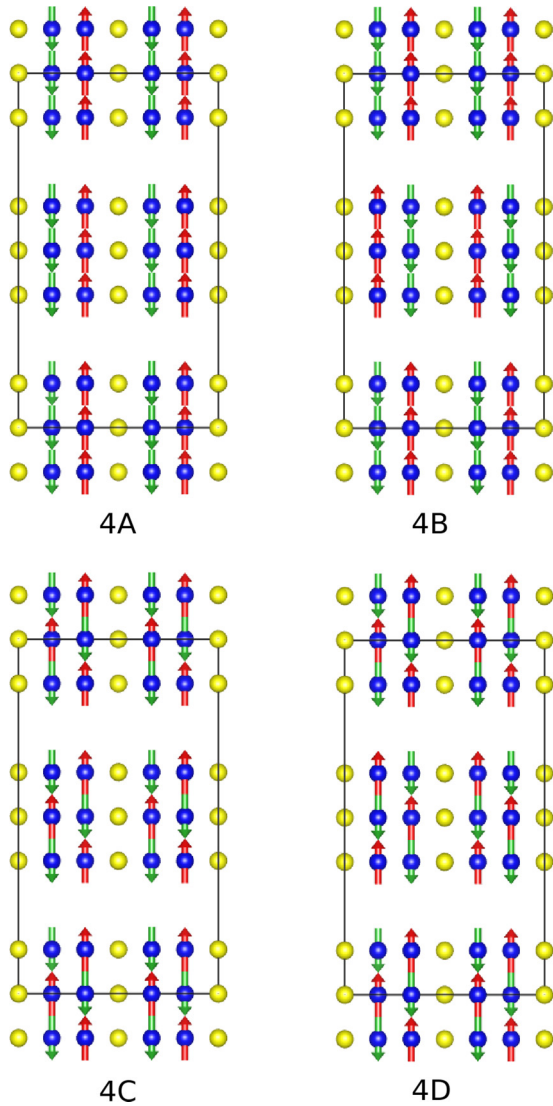$$(B4)$$

FIG. 22. AFM moment configurations A–D in $La_4Ni_3O_8$ on stripe model 4 [5]. See Fig. 8 for designations.

In our simple model $P(T_c)$ is taken to be uniform with mean T_{c0} and half-width ΔT_c:

$$P(T_c) = \begin{cases} \dfrac{1}{2\Delta T_c}, & T_c^{\min} < T_c < T_c^{\max} \\ 0 & \text{otherwise}, \end{cases} \tag{B5}$$
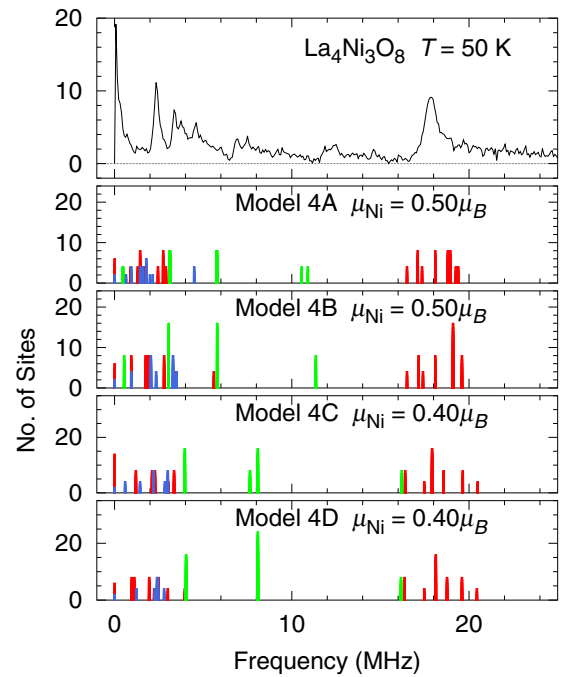
with

$$T_c^{\min (\max)} = T_{c0} \mp \Delta T_c.$$

FIG. 23. Histograms of dipolar-field μ^+ frequencies from AFM stripe models 4A–4D compared to 50-K μSR FT spectrum in $La_4Ni_3O_8$. Colors as in Fig. 9.
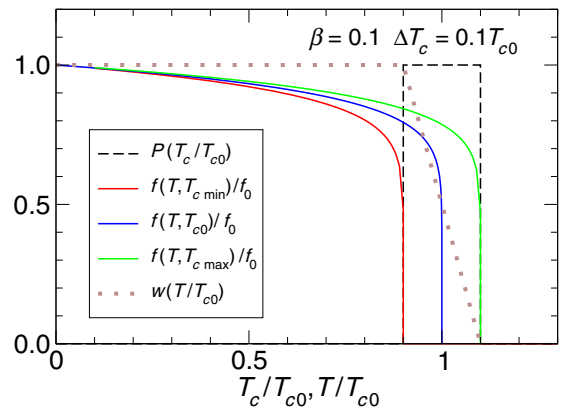

FIG. 24. Dashed curve: temperature dependence of transition temperature distribution $P(T_c)$, normalized by $2\Delta T_c$ for display. Solid curves: temperature dependencies of spontaneous NMR/NQR/μSR frequencies $f(T, T_c)$ for $T_c^{\min}$ (red), T_{c0} (blue), and $T_c^{\max}$ (green). Dotted curve: spectral weight $w(T)$.
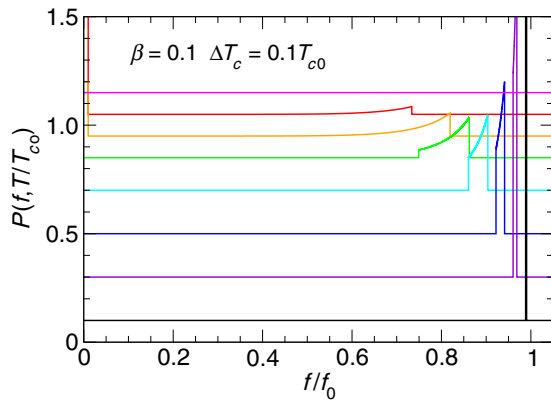
FIG. 25. Representative zero-field frequency spectra from a uniform distribution of second-order magnetic phase transition temperatures. Spectra are normalized by 0.01 for display, and are offset so that each baseline is at the corresponding temperature T/T_{c0} on the P axis. For $T > T_c^{\min}$ spectral weight is transferred from nonzero frequencies to $f = 0$.

Figure 24 shows $P(T_c)$, $f(T, T_c)$ for $T_c = T_c^{\min}$, T_{c0}, and $T_c^{\max}$, and the normalized spectral weight

$$w(T) = \begin{cases} 1 - \int_{T_c^{\min}}^{T} P(T_c)\, dT_c, & T_c^{\min} < T < T_c^{\max} \\ 1 \text{ otherwise.} \end{cases} \tag{B6}$$

The integral is the fraction $1 - w(T)$ of the sample volume with $T_c < T$, for which $f = 0$.

Representative spectra from Eq. (B4) are shown in Fig. 25. Their behavior is qualitatively similar to that of peak 6 of our experimental results in $La_4Ni_3O_8$ (Fig. 4): common features include a slight frequency decrease and loss of $f > 0$ spectral weight (transferred to $f = 0$) for $T > T_c^{\min}$. The remaining weight for $f > 0$ becomes broadly distributed, with a peak at the maximum. The shapes of the observed and calculated spectra differ, but these depend strongly on the form of the T_c distribution and would not be expected to be reproduced in this simple model. The observed peaks are broader than those of the model, probably reflecting disorder that is not taken into account in the model.

[1] J. G. Bednorz and K. A. Müller, Perovskite-type oxides–the new approach to high-T_c superconductivity, The Nobel Prize Lecture (1987).

[2] P. Lacorre, Passage from T-type to T′-type arrangement by reducing $R_4Ni_3O_{10}$ to $R_4Ni_3O_8$ (R = La, Pr, Nd), J. Solid State Chem. **97**, 495 (1992).

[3] V. V. Poltavets, K. A. Lokshin, M. Croft, T. K. Mandal, T. Egami, and M. Greenblatt, Crystal structures of $Ln_4Ni_3O_8$ (Ln = La, Nd) triple layer T′-type nickelates, Inorg. Chem. **46**, 10887 (2007).

[4] V. V. Poltavets, K. A. Lokshin, A. H. Nevidomskyy, M. Croft, T. A. Tyson, J. Hadermann, G. Van Tendeloo, T. Egami, G. Kotliar, N. ApRoberts-Warren, A. P. Dioguardi, N. J. Curro, and M. Greenblatt, Bulk Magnetic Order in a Two-Dimensional Ni^{1+}/Ni^{2+} (d^9/d^8) Nickelate, Isoelectronic with Superconducting Cuprates, Phys. Rev. Lett. **104**, 206403 (2010).

[5] J. Zhang, Y.-S. Chen, D. Phelan, H. Zheng, M. R. Norman, and J. F. Mitchell, Stacked charge stripes in the quasi-2D trilayer nickelate $La_4Ni_3O_8$, Proc. Natl. Acad. Sci. USA **113**, 8945 (2016).

[6] J. Zhang, D. M. Pajerowski, A. S. Botana, H. Zheng, L. Harriger, J. Rodriguez-Rivera, J. P. C. Ruff, N. J. Schreiber, B. Wang, Y.-S. Chen *et al.*, Spin Stripe Order in a square Planar Trilayer Nickelate, Phys. Rev. Lett. **122**, 247201 (2019).

[7] S.-H. Lee and S.-W. Cheong, Melting of Quasi-Two-Dimensional Charge Stripes in $La_{5/3}Sr_{1/3}NiO_4$, Phys. Rev. Lett. **79**, 2514 (1997).

[8] J. H. Brewer, Muon spin rotation/relaxation/resonance, in *Encyclopedia of Applied Physics*, Vol. 11, edited by G. L. Trigg, E. S. Vera, and W. Greulich (VCH, New York, 1994), pp. 23–53; S. J. Blundell, Spin-polarized muons in condensed matter physics, Contemp. Phys. **40**, 175 (1999); A. Yaouanc and P. Dalmas de Réotier, *Muon Spin Rotation, Relaxation, and Resonance: Applications to Condensed Matter*, International Series of Monographs on Physics (Oxford University Press, New York, 2011).

[9] S. Chakravarty, B. I. Halperin, and D. R. Nelson, Low-Temperature Behavior of Two-Dimensional Quantum Antiferromagnets, Phys. Rev. Lett. **60**, 1057 (1988); Two-dimensional quantum Heisenberg antiferromagnet at low temperatures, Phys. Rev. B **39**, 2344 (1989).

[10] S. Chakravarty and R. Orbach, Electron and Nuclear Magnetic Relaxation in La_2CuO_4 and Related Cuprates, Phys. Rev. Lett. **64**, 224 (1990).

[11] T. Imai, C. P. Slichter, K. Yoshimura, and K. Kosuge, Low Frequency Spin Dynamics in Undoped and Sr-Doped La_2CuO_4, Phys. Rev. Lett. **70**, 1002 (1993); T. Imai, C. P. Slichter, K. Yoshimura, M. Katoh, and K. Kosuge, High-temperature $^{63,65}Cu$ NQR and NMR study of the high-temperature superconductor $La_{2-x}Sr_xCuO_4$ ($0 \leqslant x \leqslant 0.15$), Phys. B (Amsterdam) **197**, 601 (1994).

[12] N. ApRoberts-Warren, A. P. Dioguardi, V. V. Poltavets, M. Greenblatt, P. Klavins, and N. J. Curro, Critical spin dynamics in the antiferromagnet $La_4Ni_3O_8$ from ^{139}La nuclear magnetic resonance, Phys. Rev. B **83**, 014402 (2011).

[13] V. I. Anisimov, D. Bukhvalov, and T. M. Rice, Electronic structure of possible nickelate analogs to the cuprates, Phys. Rev. B **59**, 7901 (1999).

[14] V. V. Poltavets, K. A. Lokshin, S. Dikmen, M. Croft, T. Egami, and M. Greenblatt, $La_3Ni_2O_6$: A New Double T′-type Nickelate with Infinite $Ni^{1+/2+}O_2$ Layers, J. Am. Chem. Soc. **128**, 9050 (2006).

[15] V. Pardo and W. E. Pickett, Quantum Confinement Induced Molecular Correlated Insulating State in $La_4Ni_3O_8$, Phys. Rev. Lett. **105**, 266402 (2010); Pressure-induced metal-insulator and spin-state transition in low-valence layered nickelates, Phys. Rev. B **85**, 045111 (2012).

[16] S. Sarkar, I. Dasgupta, M. Greenblatt, and T. Saha-Dasgupta, Electronic and magnetic structures of bilayer $La_3Ni_2O_6$ and trilayer $La_4Ni_3O_8$ nickelates from first principles, Phys. Rev. B **84**, 180411(R) (2011).

[17] J.-G. Cheng, J.-S. Zhou, J. B. Goodenough, H. D. Zhou, K. Matsubayashi, Y. Uwatoko, P. P. Kong, C. Q. Jin, W. G. Yang, and G. Y. Shen, Pressure Effect on the Structural Transition and Suppression of the High-Spin State in the Triple-Layer T'-La$_4$Ni$_3$O$_8$, Phys. Rev. Lett. **108**, 236403 (2012).

[18] T. Liu, G. Zhang, X. Zhang, T. Jia, Z. Zeng, and H. Q. Lin, Electronic structure and magnetism of La$_4$Ni$_3$O$_8$ from first principles, J. Phys.: Condens. Matter **24**, 405502 (2012).

[19] H. Wu, Charge-spin-orbital states in the tri-layered nickelate La$_4$Ni$_3$O$_8$: an ab initio study, New J. Phys. **15**, 023038 (2013).

[20] L. Patra, M. Ashwin Kishore, R. Vidya, A. O. Sjåstad, H. Fjellvåg, and P. Ravindran, Electronic and magnetic structures of hole doped trilayer La$_{4-x}$Sr$_x$Ni$_3$O$_8$ from first-principles calculations, Inorg. Chem. **55**, 11898 (2016).

[21] T. Liu, H. Wu, T. Jia, X. Zhang, Z. Zeng, H. Q. Lin, and X. G. Li, Dimensionality-induced insulator-metal crossover in layered nickelates La$_{n+1}$Ni$_n$O$_{2n+2}$ ($n = 2$, 3, and ∞), AIP Adv. **4**, 047132 (2014).

[22] N. apRoberts-Warren, J. Crocker, A. P. Dioguardi, K. R. Shirer, V. V. Poltavets, M. Greenblatt, P. Klavins, and N. J. Curro, NMR evidence for spin fluctuations in the bilayer nickelate La$_3$Ni$_2$O$_6$, Phys. Rev. B **88**, 075124 (2013).

[23] A. S. Botana, V. Pardo, W. E. Pickett, and M. R. Norman, Charge ordering in Ni^{1+}/Ni^{2+} nickelates: La$_4$Ni$_3$O$_8$ and La$_3$Ni$_2$O$_6$, Phys. Rev. B **94**, 081105(R) (2016).

[24] A. Suter and B. Wojek, MUSRFIT: A Free Platform-Independent Framework for μSR Data Analysis, Phys. Procedia **30**, 69 (2012), 12th International Conference on Muon Spin Rotation, Relaxation and Resonance (μSR2011).

[25] For a review, see P. Bonfà and R. De Renzi, Toward the computational prediction of muon sites and interaction parameters, J. Phys. Soc. Jpn. **85**, 091014 (2016).

[26] R. Kubo and T. Toyabe, A stochastic model for low field resonance and relaxation, in *Magnetic Resonance and Relaxation*, edited by R. Blinc (North-Holland, Amsterdam, 1967), pp. 810–823; R. S. Hayano, Y. J. Uemura, J. Imazato, N. Nishida, T. Yamazaki, and R. Kubo, Zero- and low-field spin relaxation studied by positive muons, Phys. Rev. B **20**, 850 (1979).

[27] Y. J. Uemura, K. Nishiyama, T. Yamazaki, and R. Nakai, Muon spin relaxation in a spin glass CuMn observed in finite longitudinal magnetic fields, Solid State Commun. **39**, 461 (1981); Y. J. Uemura, T. Yamazaki, D. R. Harshman, M. Senba, and E. J. Ansaldo, Muon-spin relaxation in AuFe and CuMn spin glasses, Phys. Rev. B **31**, 546 (1985).

[28] D. R. Noakes and G. M. Kalvius, Anomalous zero-field muon spin relaxation in highly disordered magnets, Phys. Rev. B **56**, 2352 (1997).

[29] A. Keren, P. Mendels, I. A. Campbell, and J. Lord, Probing the Spin-Dynamical Autocorrelation Function in a Spin Glass Above T_g Via Muon Spin Relaxation, Phys. Rev. Lett. **77**, 1386 (1996).

[30] D. C. Johnston, Stretched exponential relaxation arising from a continuous sum of exponential decays, Phys. Rev. B **74**, 184430 (2006).

[31] D. Tse and S. R. Hartmann, Nuclear Spin-Lattice Relaxation Via Paramagnetic Centers Without Spin Diffusion, Phys. Rev. Lett. **21**, 511 (1968).

[32] T. Moriya and K. Ueda, Nuclear magnetic relaxation in weakly ferro- and antiferromagnetic metals, Solid State Commun. **15**, 169 (1974).

[33] A. J. Millis, H. Monien, and D. Pines, Phenomenological model of nuclear relaxation in the normal state of YBa$_2$Cu$_3$O$_7$, Phys. Rev. B **42**, 167 (1990).

[34] D. E. MacLaughlin, J. P. Vithayathil, H. B. Brom, J. C. J. M. de Rooy, P. C. Hammel, P. C. Canfield, A. P. Reyes, Z. Fisk, J. D. Thompson, and S.-W. Cheong, Abrupt but Continuous Antiferromagnetic Phase Transition in Nearly Stoichiometric La$_2$CuO$_{4+\delta}$, Phys. Rev. Lett. **72**, 760 (1994).

[35] P. Imbert, G. Jéhanno, and J. A. Hodges, Comment on "Magnetization and Spin-Wave Velocities in La$_2$CuO$_4$", Phys. Rev. Lett. **71**, 654 (1993).

[36] K. H. Chow, P. A. Pattenden, S. J. Blundell, W. Hayes, F. L. Pratt, T. Jestädt, M. A. Green, J. E. Millburn, M. J. Rosseinsky, B. Hitti, S. R. Dunsiger, R. F. Kiefl, C. Chen, and A. J. S. Chowdhury, Muon-spin-relaxation studies of magnetic order in heavily doped La$_{2-x}$Sr$_x$NiO$_{4+\delta}$, Phys. Rev. B **53**, R14725 (1996).

[37] T. Jestädt, K. H. Chow, S. J. Blundell, W. Hayes, F. L. Pratt, B. W. Lovett, M. A. Green, J. E. Millburn, and M. J. Rosseinsky, Temperature and doping-level dependence of magnetic order in La$_{2-x}$Sr$_x$NiO$_{4+\delta}$ studied by muon spin rotation, Phys. Rev. B **59**, 3775 (1999).

[38] H.-H. Klauss, Spin stripe order and superconductivity in layered transition metal oxides, J. Phys.: Condens. Matter **16**, S4457 (2004).

[39] V. A. Borodin, V. D. Doroshev, Yu. M. Ivanchenko, M. M. Savosta, and A. E. Filippov, La$_2$CuO$_4$ in the fluctuation region of the magnetic transition, Pis'ma Zh. Eksp. Teor. Fiz. **52**, 1073 (1990) [JETP Lett. **52**, 469 (1990)].

[40] Y. J. Uemura, W. J. Kossler, X. H. Yu, J. R. Kempton, H. E. Schone, D. Opie, C. E. Stronach, D. C. Johnston, M. S. Alvarez, and D. P. Goshorn, Antiferromagnetism of La$_2$CuO$_{4-y}$ Studied by Muon-Spin Rotation, Phys. Rev. Lett. **59**, 1045 (1987).

[41] H. Tang, G. Xiao, A. Singh, Z. Tešanović, C. L. Chien, and J. C. Walker, Magnetic dynamics of La$_2$CuO$_4$ studied by Mössbauer spectroscopy, J. Appl. Phys. **67**, 4518 (1990).

[42] T. Imai, S. K. Takahashi, A. Arsenault, A. W. Acton, D. Lee, W. He, Y. S. Lee, and M. Fujita, Revisiting ^{63}Cu NMR evidence for charge order in superconducting La$_{1.885}$Sr$_{0.115}$CuO$_4$, Phys. Rev. B **96**, 224508 (2017).

[43] A. Arsenault, S. K. Takahashi, T. Imai, W. He, Y. S. Lee, and M. Fujita, ^{139}La NMR investigation of the charge and spin order in a La$_{1.885}$Sr$_{0.115}$CuO$_4$ single crystal, Phys. Rev. B **97**, 064511 (2018).

[44] T. Imai and Y. S. Lee, ^{139}La and ^{63}Cu NMR investigation of charge order in La$_2$CuO$_{4+y}$ ($T_c = 42$ K), Phys. Rev. B **97**, 104506 (2018).